

DESY Summer Student Programme 2012

Study of the properties of photon candidates in the Higgs to gamma gamma search

Skorda Eleni

Supervisor: Marcos Jimenez

Abstract

With the latest results from the ATLAS collaboration, it is becoming more and more apparent, that the $H \rightarrow \gamma\gamma$ is valuable from experimental point of view. In this project, the $H \rightarrow \gamma\gamma$ was reproduced using 2011 data and the main outline is presented. The calorimetric properties of the photon candidates are studied in the region where the resonance was observed and compared with the background regions.



ARISTOTLE UNIVERSITY
OF THESSALONIKI

Hamburg, DESY, September 7, 2012

Contents

1	Introduction	2
2	ATLAS Detector	3
3	Photon Reconstruction	4
4	Event Selection	6
5	Comparison of photon properties in the signal and side-band regions	7
6	Conclusions	9
7	Aknowledgements	9

1 Introduction

Reproducing the $H \rightarrow \gamma\gamma$ analysis using 2011 data was one of the main goals of this project. To achieve agreement with the analysis, certain selection criteria were applied to 2011 data. The second objective was to study the event level distribution (invariant mass, p_T , η , ϕ , etc.) and the properties of different categories of photon candidates in the $H \rightarrow \gamma\gamma$ search. Software development, that would serve the purposes of these studies was also a significant part of this project. In order to determine if the observed signal was actual photons, signal and side-band regions were defined and the properties of the photons in these regions were compared.

In order to explain how the W and Z acquire mass in the Standard Model (SM), a scalar Higgs field is introduced, the quanta of which is the hypothetical Higgs boson. The Higgs field has a degenerate vacuum inducing the spontaneous breaking of electroweak symmetry, the mechanism whereby the W and Z bosons acquire mass. This process is referred to as the "Higgs mechanism".

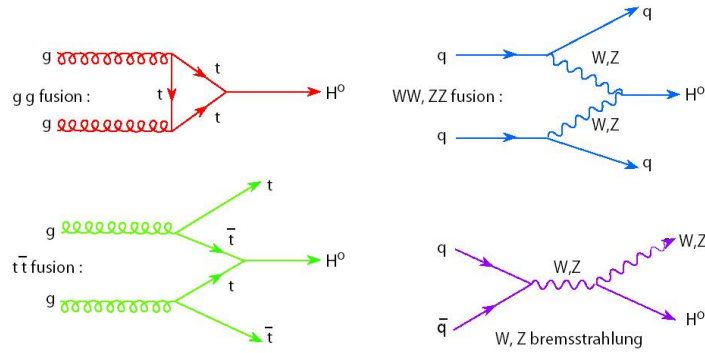


Figure 1: Feynman diagrams for standard model Higgs production mechanisms

The main SM production mechanisms are shown in figure 1 for pp collisions and they are: gluon fusion, weak gauge boson fusion and top quark fusion. The dominant production process is gluon fusion. Figure 2 shows the branching ratio fraction in different final states as a function of Higgs mass. The branching ratio is given by $B_i = \frac{\Gamma_i}{\Gamma}$ where Γ_i is the width in one decay channel and Γ is the total width. $H \rightarrow \gamma\gamma$ has lower branching ratio than other channels. The signal of Higgs production in this channel would be observed in the di-photon invariant mass distribution as a very narrow resonance on top of an exponentially decaying background. This easily identifiable signal makes this channel valuable from an experimental point of view, despite the expected low branching fraction. The latest results from the ATLAS Collaboration using roughly $11 fb^{-1}$ of combined 7 and 8 TeV pp collision data find evidence for the presence of a resonance at 126 GeV consistent with the SM Higgs boson [3].

The exponential distribution of the background gives in the signal region a narrow resonance. In this aspect this channel is rare but clean for a low-mass Higgs search.

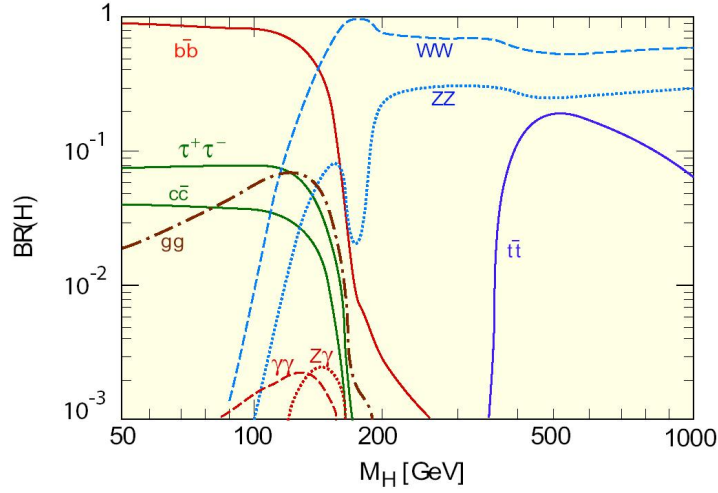


Figure 2: Branching Ratio Graphs for Higgs decay channels

2 ATLAS Detector

The ATLAS detector is a multipurpose detector designed for physics studies at the LHC. It is built in several concentric cylindric layers around the beam interaction point. It can be divided into four main parts, which are the inner detector, the calorimeters, the muon spectrometer and the magnet system. An overall design of ATLAS detector is shown in figure 3. The inner detector is used to measure the momentum of the charged particles. The calorimeters are used for measuring particles' energy deposits, whereas the muon spectrometer identifies muons and measures their momenta. The magnet system is used to bend charged particles' tracks in the inner detector and in the muon spectrometer, allowing momenta measurements.

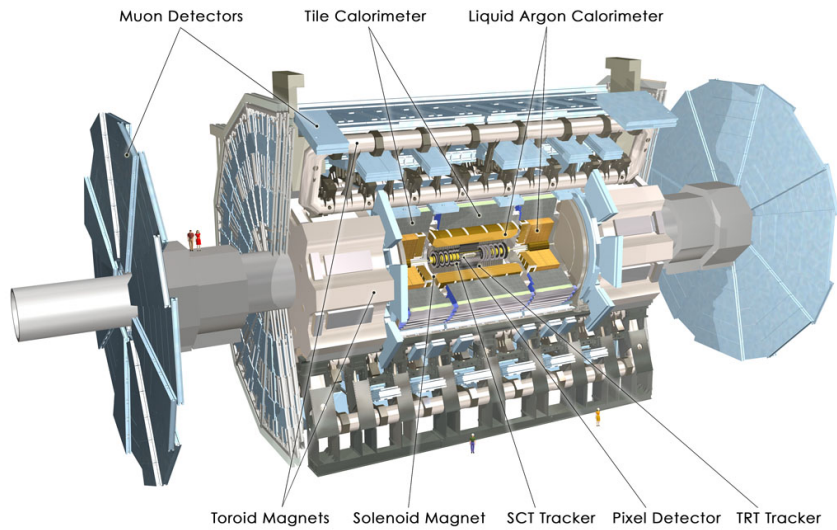


Figure 3: ATLAS detector.

There are two calorimeter systems. The innermost is the electromagnetic calorime-

ter which is surrounded by the hadronic calorimeter. Electromagnetic calorimeter is a sampling calorimeter, which means that it is built by assembling layers of passive material (lead) alternated with layers of active material (liquid argon). The particles interact with the passive material and a shower of particles is created and detected by the active material.

The main tasks of the electromagnetic calorimeter is to measure the energy deposit of electrons and photons and to identify them against the hadrons. Identification is made possible by the information we obtain on the longitudinal and the lateral development of the shower and is essential for determining the impact position on the calorimeter and for giving the photon direction. The electrodes are divided longitudinally into three parts, each one sampling a part of the shower energy. The depth of each one varies in η and are named front (strips), middle and back as shown in figure 4. In the middle the bulk of the shower's energy is measured. In the back segmentation the tail of the shower is measured. The front (strips) is eight times more segmented in η and 5 times coarser in ϕ . The longitudinal segmentation of the calorimeter and its fine segmentation in ϕ offers improved identification of π_0 and measurement of the direction of showers. The endcap calorimeters have similar geometry.

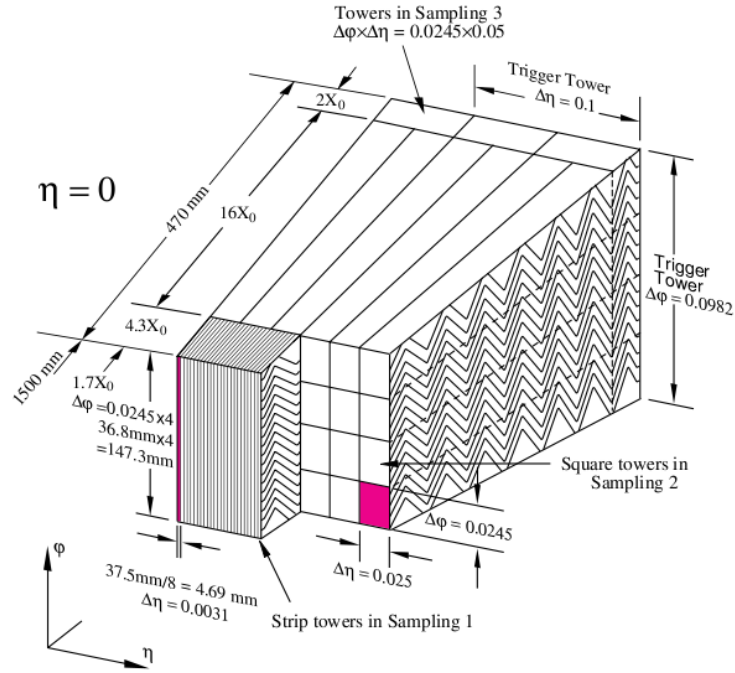


Figure 4: ATLAS ECAL.

3 Photon Reconstruction

There are three levels in the ATLAS triggering system and these are: the first level trigger, the Level-2 (L2) trigger and the Event Filter (EF). The trigger uses sliding window algorithm to select photon candidates. Trigger also applies some loose selection criteria on the shape of the shower. After photon candidates are reconstructed, they are

used in analysis where a tight selection is applied. There are two types of reconstructed photons: converted and unconverted photons.

Photon candidates are identified offline through a dedicated cut-based selection based on the shower shapes of the electromagnetic clusters in the EMC. The variables that are used for loose and tight identification are showed in the following table 6.

After the photons are produced they have to travel a substantial amount of material, meaning there is a probability for the photon to convert to an electron-positron pair before it reaches the electromagnetic calorimeter. In figure 5 the converted photons are plotted as a function of η . In η regions with less detector material, there are more unconverted photons and vice-versa for converted.

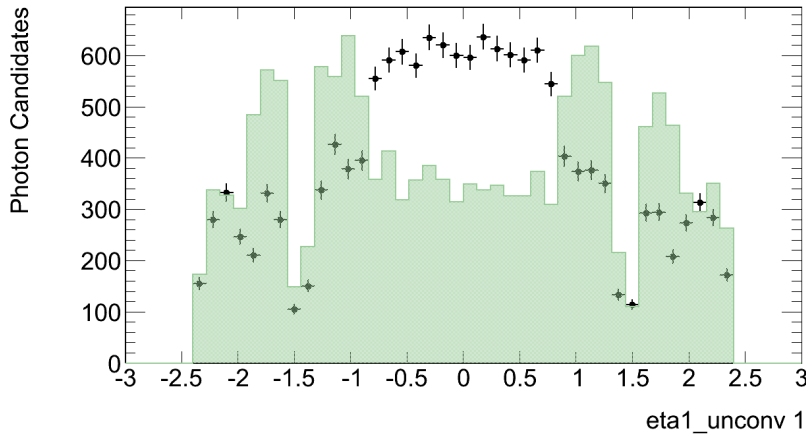


Figure 5: Eta distribution for converted and unconverted photons. Converted photons are signed with green color and inconverted photons with black dots

If there is a track originating from a vertex inside the inner detector which matches an a electromagnetic cluster, then the cluster object is flagged as a converted photon. The track is considered to match an electromagnetic cluster if its its impact point after extrapolation from the second sampling of the calorimeter is within a certain range in (η, ϕ) from the cluster center. If there are no associated tracks and there is only the energy deposit in the calorimeter the photon candidate is reconstructed as a converted photon.

The trajectories of the photons are essential to be reconstructed well, because the opening angle between the two photons is used to calculate the invariant mass of the photon pair according to the following equation.

$$M^2 = 2p_{T1}p_{T2}(\cosh(\eta_1 - \eta_2) - \cos(\phi_1 - \phi_2))$$

The variables that are used for loose and tight identification are showed in the following table 6. The calorimetric variables used in the photon selections and are studied are variables that use the second longitudinal compartment (middle layer) of the electromagnetic calorimeter (EMC), and those that use the first longitudinal compartment (strip layer) of the EMC. Those from the front layer, due to fine segmented strips, are used to study in detail the structure of the shower and provide higher discrimination power.

Category	Description	Name	Loose	Tight
Acceptance	$ \eta < 2.37, 1.37 < \eta < 1.52$ excluded	–		✓
Hadronic leakage	Ratio of E_T in the first sampling of the hadronic calorimeter to E_T of the EM cluster (used over the range $ \eta < 0.8$ and $ \eta > 1.37$)	R_{had_1}	✓	✓
	Ratio of E_T in all the hadronic calorimeter to E_T of the EM cluster (used over the range $0.8 < \eta < 1.37$)	R_{had}	✓	✓
EM Middle layer	Ratio in η of cell energies in 3×7 versus 7×7 cells	R_η	✓	✓
	Lateral width of the shower	w_2	✓	✓
	Ratio in ϕ of cell energies in 3×3 and 3×7 cells	R_ϕ		✓
EM Strip layer	Shower width for three strips around maximum strip	w_{s3}		✓
	Total lateral shower width	$w_{s\text{tot}}$		✓
	Fraction of energy outside core of three central strips but within seven strips	F_{side}		✓
	Difference between the energy associated with the second maximum in the strip layer, and the energy reconstructed in the strip with the minimal value found between the first and second maxima	ΔE		✓
	Ratio of the energy difference associated with the largest and second largest energy deposits over the sum of these energies	E_{ratio}		✓

Figure 6: variables used for loose and tight selection

4 Event Selection

In the $H \rightarrow \gamma\gamma$ analysis that was performed for this project, specific selection criteria were applied. The selected events were requested to have least one primary vertex. The photons should be in the fiducial region $|\eta| < 2.37$ $1.37 < |\eta| < 1.52$ of the detector excluded the crack regions. The candidates are required to be isolated by having at most 4 GeV of energy deposited in the calorimeter in a cone $\Delta R \sim 0.4$ around them. Kinematic criteria were also requested. The leading photon $p_T > 40$ GeV and sub-leading photon $p_T > 30$ GeV. Tight selection is also applied (refer to table 6). The invariant mass of the two photons is shown in figure 7. In figure 8 are shown the p_T and η distributions of the leading photons.

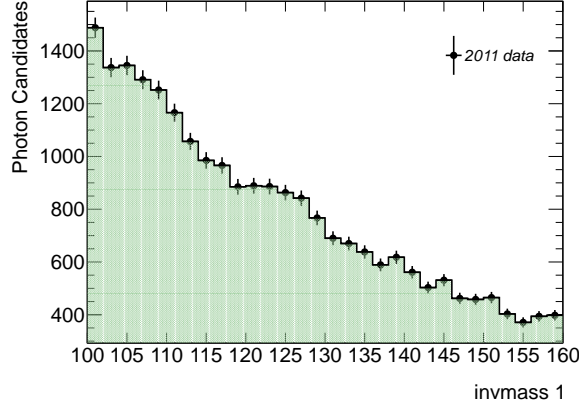


Figure 7: variables used for loose and tight selection

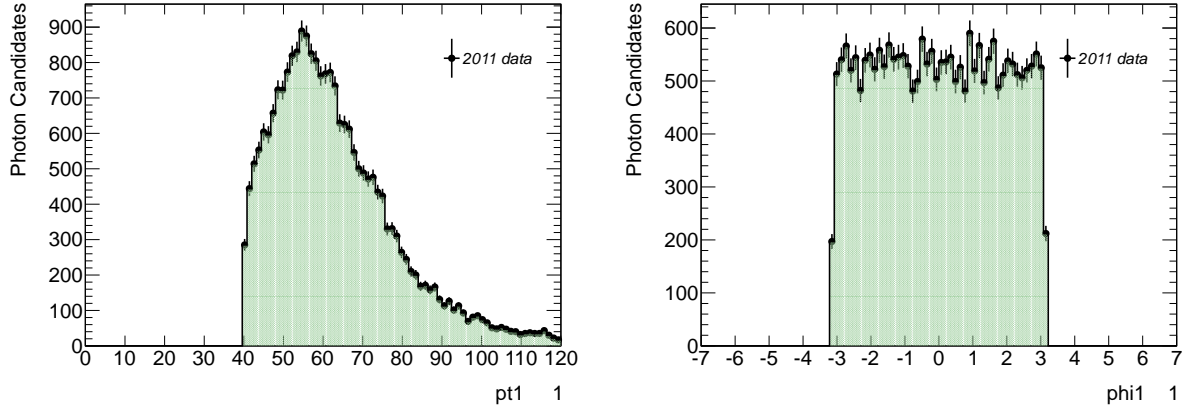


Figure 8: pt and eta distributions for leading photons

Background events SM predicts diphoton production, which induces irreducible background in $H \rightarrow \gamma\gamma$ search. Misidentified jets (one or two) also consist background for this analysis, but this background is reducible. Finally, a fraction background is caused by the Drell-Yan processes.

5 Comparison of photon properties in the signal and side-band regions

In the current analysis in the signal region are considered the photons with invariant mass between 122 and 128 GeV and as side-band photons with invariant mass below 122 and above 128 GeV. As it was mentioned before it is interesting to compare the behaviour. The variables described in sec. 3 for discriminating fake photons can be used to study the properties of the photons in the signal region. It is expected that photons in the signal region have the same distributions with photons in the side band. Differences in the distributions would indicate that in the resonance region there are no an actual photons but objects faking photons, which could be signal for new physics.

Distributions of the calorimetric discriminating variables for signal and side-band region are shown in figure 10 for converted photons and in figure 9 for unconverted.

In the distributions of the discriminating variables no deviation is observed from the photon-like signal in the resonance region, at this level of detail.

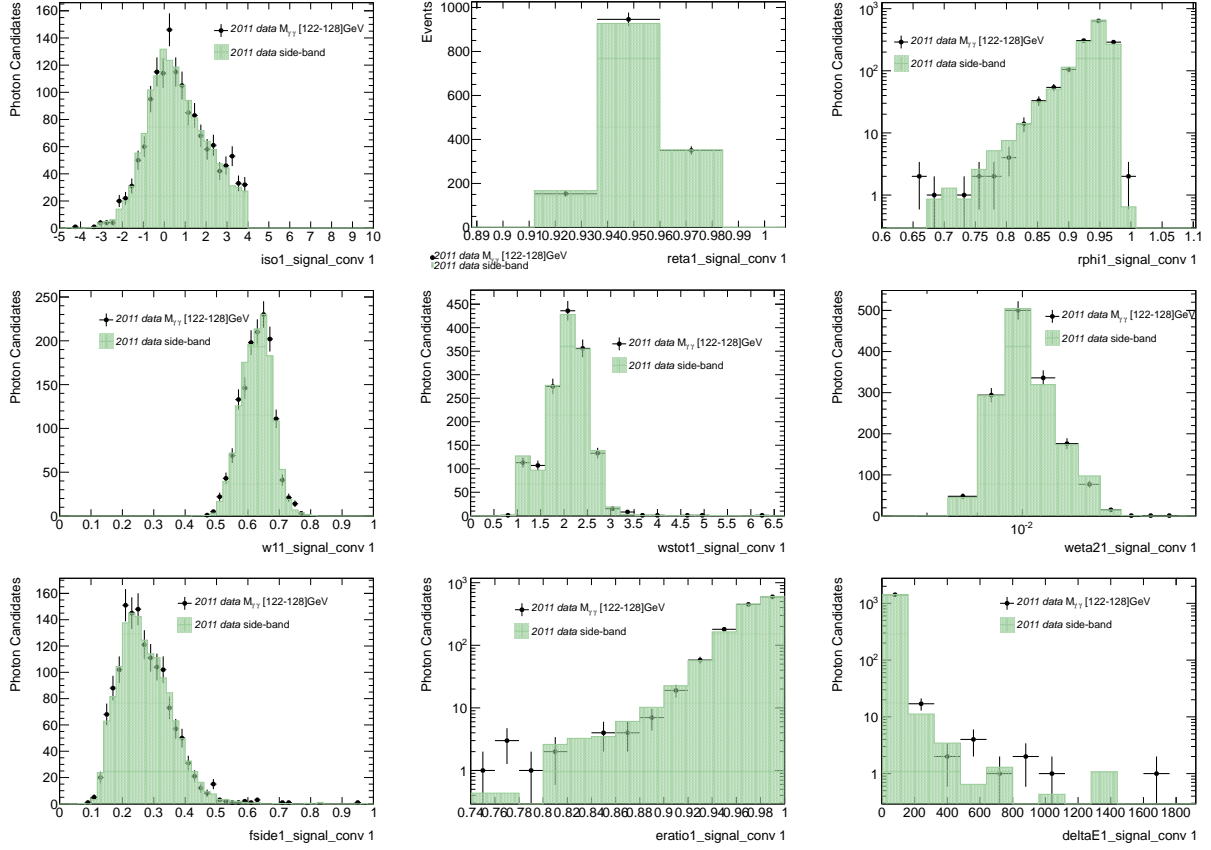


Figure 9: Shower shape distributions for converted photons.

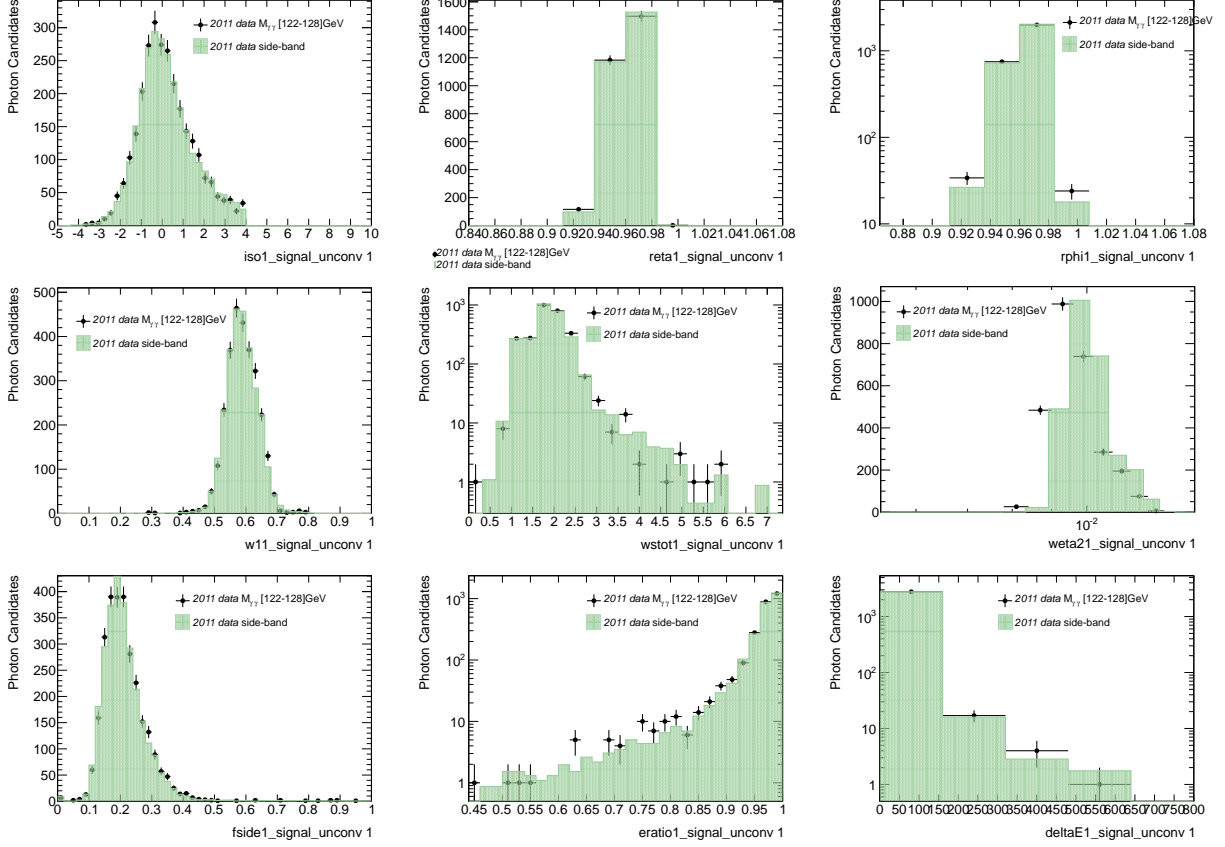


Figure 10: Shower shape distributions for unconverted photons.

6 Conclusions

A good level of agreement was achieved with the 2011 data analysis. In the level of detail that this study allowed no difference was observed in the distributions of the discriminating variables. Now that all the necessary tools needed are set-up and ready to be used for more detailed studies of the distributions can be performed.

7 Acknowledgements

I would like to thank DESY summer student program and Higgs to gamma gamma group at DESY for giving me the opportunity to work on this project. I would specially like to thank my supervisor Marcos Jimenez, Kerstin Tackmann, Sergey Gleyser and Christopher Hengler for all their help and advice.

References

- [1] Expected photon performance in the ATLAS experiment *The Atlas Colaboration*
- [2] Search for the Standard Model Higgs boson in the diphoton decay channel with 4.9 fb^{-1} of pp collision data at $\sqrt{s} = 7$ TeV with ATLAS *The Atlas Colaboration*
- [3] High Energy Physics - Experiment Observation of a new particle in the search for the Standard Model Higgs boson with the ATLAS detector at the LHC *The Atlas Colaboration*